Physical Characteristic and Molecular Structure of Spin-Crossover Iron(III) Complexes of Monoclinic Form with Hexadentate Ligands Derived from Triethylenetetramine and Salicylaldehyde [Fe(sal$_2$trien)]BPh$_4$·acetone

Yonezo MAEDA,* Hiroki OSHIO,† Yuichi TANIGAWA, Takayuki ONIKI,†† and Yoshimasa TAKASHIMA
Department of Chemistry, Faculty of Science, Kyushu University, Hakozaki, Higashiku, Fukuoka 812
† The Institute for Molecular Science, Okazaki, Aichi 444
†† Kyushu Dental College, Tokuyoshi, Kokuraminamiku, Kitakyushu 803-02
(Received October 18, 1990)

Iron(III) complexes of [FeL]BPh$_4$·acetone containing the hexadentate ligand derived from triethylenetetramine and salicylaldehyde have been synthesized. These complexes were grown in two crystalline forms, monoclinic and the twin crystals. The crystal structure of the monoclinic form was determined at 290 K, at which temperature the complex is in a transition spin-state between high- and low-spin states; the spin-state interconversion rate of the monoclinic form is as fast as the inverse of the Mössbauer lifetime (1×10^{-7} s) above 200 K. The monoclinic crystal of [FeL]BPh$_4$·acetone is of space group $P2_1/a$, with a=27.418(4), b=10.097(2), c=14.726(3) Å, β=98.00(1)°, and Z=4. The average bond distances of Fe–O (1.875 Å), Fe–N_{imine} (1.988 Å), and Fe–N_{amine} (2.069 Å) are in good agreement with the expected values for the transition spin-state between high- and low-spin states. Twin crystals are in a high-spin state over the temperature range 78—320 K.

The dynamics of spin-state interconversion in a solution and a solid at ambient temperature have been the subject of a number of papers.[1-3] The measured ^{2}T(LS)$\rightleftharpoons$ ^{6}A(HS) relaxation rates are of the order of 10^7 s^{-1} in the solution state at high temperature; there are few solids for which both the solution and solid-state spin-state interconversion rates have been determined.[4,5] The solid-state rates are supposed to be consistently slower than the corresponding solution rates.

The spin-state interconversion rates in [FeL]Y (H_2L; Schiff base derived from triethylenetetramine and salicylaldehyde) with Y=PF_6^-, NO_3^-, BPh_4^-, I^-, and Cl^- in solution were measured by Tweedle and Wilson, and are about 10^7 s^{-1}.[5] The magnetic properties and the crystal structures for some of their solid complexes have been reported and the interconversion rate for the PF_6 salt has been estimated to be slower than 10^7 s^{-1}.[6]

Some examples in which the electronic spin-state is dependent on the crystal form are known. For example, Fe(phen)$_2$(NCS)$_2$ and Fe(bpy)$_2$(NCS)$_2$ have polymorph,[7-9] and the magnetic behaviors are different from each other. [Fe(oep)(3-Clpy)$_2$]ClO_4[10,11] (oep: octaethylporphyrin, 3-Clpy: 3-chloropyridine) of monoclinic form is a quantum-admixed intermediate-spin state; the triclinic one shows a thermal spin equilibrium, although the solution susceptibilities of both crystalline forms are identical.

We are interested in the differences in the spin-state interconversion rates between the solution- and solid-state, and in the effect of the difference of the crystal forms on the spin-crossover.

Experimental

Sample Preparation. The ligand was prepared by slowler adding 0.73 g (5 mmol) of triethylenetetramine in 20 ml of methanol to 1.22 g (10 mmol) of salicylaldehyde in 100 ml of methanol; the mixture was kept for 1 h at room temperature.[12] Then, 1.12 g (20 mmol) of KOH in 50 ml of methanol was added to the mixture. This mixture was used without separating the ligand as a solid. Iron complexes were prepared by the addition of 2.0 g (5 mmol) of iron nitrate in 50 ml of methanol to the ligand solution. The precipitation was separated with a glassfilter and 1.36 g (4 mmol) of sodium tetraphenylborate in 50 ml of methanol was slowly poured into the filtrate. The crude product was collected by filtration, washed with methanol and recrystallized from acetone. Two crystal forms were produced, filtrated, washed with acetone and separated mechanically. The crystals of each form were collected and recrystallized from acetone. The analytical data for [FeL]BPh$_4$·acetone are as follows: Found for monoclinic crystals: C, 72.01; H, 6.40; N, 7.15%. Found for twin crystals: C, 71.93; H, 6.51; N, 7.23%. Calcd for $BC_{47}H_{50}FeN_4O_3$: C, 71.85; H, 6.42; N, 7.13%.

Physical Measurements. The magnetic susceptibilities of the polycrystalline samples were measured by the Faraday method using a type-2002 (Cahn Instruments) electrobalance with an electromagnet (8000 G, 0.8 T). The temperature was controlled over the range 78—320 K by using a digital temperature controller (model 3700; Scientific Instruments). Compound $HgCo(NCS)_4$ was used as a calibration standard. Effective magnetic moments were calculated by using the formula $\mu_{eff}=2.84\,(\chi_M T)^{1/2}$, where χ_M is the molar susceptibilities after applying a diamagnetic correction.

The Mössbauer spectra were measured with a constant-acceleration spectrometer (Austin Science Associates). Data were stored in a 1024-channel pulse-height analyzer (type 5200; Inotech Inc.). The temperature was monitored with a calibrated copper–constantan thermocouple within a variable-temperature cryostat (type ASAD-4V). A cobalt 57 source of 10 mCi diffused into a palladium foil was used for the absorption measurement. All spectra were fitted by Lorentzian line shapes using a least-squares fitting procedure at the Computer Center, Kyushu university. The velocity scale was normalized with respect to the centre of the spectrum of metallic iron at 296 K.

The relaxation fits were based on the method reported in Ref. 13 for relaxation between two quadrupole split doublets representing the low- and high-spin electronic states. The quadrupole splittings of the low- and high-spin doublets in these fits were kept constant at 2.85 and 0.28 mm s^{-1}, respectively. The high- and low-spin population fractions determined from the magnetic data were used. We used values of 2.58 BM for the low-spin electronic state and 5.60 BM for high-spin electronic state, of which value is popularly observed for high-spin iron(III) complexes. The line widths for the doublets were assumed to be 3.03 mm s^{-1} for the low-energy line 0.86 mm s^{-1} for the high-energy line of the high-spin species; those for low-spin species were 0.44 and 0.31 mm s^{-1}, respectively. The values were varied according to the fraction of the high-spin/low-spin population in fitting as inevitable management, since the high-spin species shows very broad line widths due to spin–spin relaxation. (The values used in practice for fitting were less than 2.199 mm s^{-1}, although 3.03 mm s^{-1} appeared to be too large.)

The IR spectra for both samples were measured using a JASCO FT/IR-5000; the peak positions of N–H or C=N stretching vibration for monoclinic crystals (complex **a**) were similar to those for the twin crystals. No existence of strong hydrogen bonding in N(2)–H(23)–OS(1) is supposed for both complexes.

Electron paramagnetic resonance data at the X-band frequency were collected on a FEX (JEOL, Ltd) spectrometer.

Crystal Structure Determination of Monoclinic [Fe(sal$_2$trien)]BPh$_4$·acetone. Suitable single crystals of monoclinic [FeL]BPh$_4$·acetone were obtained by slow evaporation of acetone at room temperature.

Crystal Data. $BC_{47}H_{50}FeN_4O_3$, M=785.5. Monoclinic, a=27.418(4), b=10.097(2), c=14.726(3)A, β=98.00(1)°, V=4037(0)Å^3 (by least squares refinement on diffractomer angles $25°<2\theta<30°$ for 50 automatically centered reflections, λ=0.71073 Å), space group $P2_1/a$ (No. 14), Z=4, D_c=1.29 g cm^{-3}, D_o=1.30 g cm^{-3}, blue black, crystal dimensions: 0.2×0.2×0.3 mm, μ(Mo $K\alpha$)=16.46 cm^{-1}.

Data Collection and Processing. Diffraction data were collected at 290 K on a Rigaku AFC5 four-circle diffractometer using the $\omega-2\theta$ scan technique; graphite monochromated Mo $K\alpha$ radiation; 10333 reflections measured($-35<h<35$, $0<k<13$, $0<l<19$), 5287 independent data with $|F_o|>3\sigma(F_o)$. The crystal was covered with glue in order to avoid any release of acetone molecules from the crystal during measurements. The intensities of the three standard reflection were monitored every 100 reflections, and showed no greater fluctuations during the data collection than that expected from Poisson statistics. Intensity data were corrected for both Lorentz and polarization factors, but not for adsorption and extinction.

Structure Analysis and Refinement. The structure was solved by the conventional heavy-atom method and refined by a block-diagonal least-squares method with anisotropic thermal parameters for non-hydrogen atoms and isotropic for Hydrogen atoms. The weighting scheme $w=[\sigma_c^2+(0.025|F_o|)^2]^{-1}$ was employed, where σ_c was estimated from the counting statistics. The final indices, R and R', were 7.2 and 9.3%, respectively, which are defined as $R=\Sigma(|F_o|-|F_c|)/\Sigma|F_o|$ and $R'=[\Sigma w(|F_o|-|F_c|)^2/\Sigma w|F_o|^2]^{1/2}$. The atomic scattering factors for non-hydrogen atoms were taken from Ref. 14, and those for hydrogen atoms from Stewart et al.[15] The effects of anomalous scattering for non-hydrogen atoms were corrected for in structure factor calculations. A determination of the structural parameters was carried out with the universal Crystallographic Computation Program System UNICS III,[16] using a HITAC M-680 Computer at the Computer Center of The Institute for Molecular Science. The final atomic coordinates are given in Table 1.

Table 1. Positional Parameters of the Cation and Acetone Molecule for Monoclinic [Fe(sal$_2$trien)]BPh$_4$·acetone with Estimated Standard Deviations in Parentheses (×10^5 for Fe and ×10^4 for the Other Atoms)

Atom	x	y	z
Fe	12683 (3)	8787 (7)	20157 (5)
O(1)	1167 (1)	−904 (4)	1687 (2)
O(2)	650 (1)	1292 (4)	2348 (2)
N(1)	1034 (2)	1450 (4)	734 (3)
N(2)	1469 (2)	2847 (4)	2156 (3)
N(3)	2003 (2)	682 (5)	1847 (4)
N(4)	1526 (2)	375 (5)	3293 (3)
C(1)	881 (2)	−1422 (5)	975 (4)
C(2)	778 (2)	−2765 (5)	964 (4)
C(3)	492 (2)	−3353 (6)	247 (5)
C(4)	290 (2)	−2613 (7)	−505 (4)
C(5)	387 (2)	−1296 (7)	−536 (4)
C(6)	685 (2)	−655 (5)	202 (3)
C(7)	782 (2)	720 (5)	112 (3)
C(8)	1110 (3)	2861 (6)	538 (4)
C(9)	1154 (2)	3595 (6)	1422 (4)
C(10)	2015 (2)	3037 (6)	2183 (4)
C(11)	2221 (2)	1956 (7)	1645 (5)
C(12)	2253 (3)	62 (10)	2663 (9)
C(13)	2021 (3)	−163 (12)	3415 (5)
C(14)	1302 (2)	500 (5)	4005 (4)
C(15)	811 (2)	1014 (5)	3983 (3)
C(16)	628 (2)	1121 (6)	4822 (4)
C(17)	167 (2)	1555 (7)	4875 (4)
C(18)	−131 (2)	1895 (6)	4079 (4)
C(19)	36 (2)	1815 (6)	3240 (4)
C(20)	515 (2)	1355 (5)	3169 (3)
OS(1)	1202 (2)	4969 (6)	3376 (4)
CS(1)	937 (3)	5665 (6)	3747 (4)
CS(2)	981 (3)	7114 (7)	3755 (5)
CS(3)	572 (4)	5088 (9)	4299 (8)

Results and Discussion

We isolated solids of two crystalline forms with a solvent. The temperature-dependent magnetic susceptibilities for the two crystalline forms were different from each other. The crystal structure of the monoclinic form, which shows thermal spin-crossover, was determined. Twin crystals give a different powder X-ray diffraction pattern from the monoclinic one and are in a high-spin state over the temperature range 78–320 K.

Magnetic Susceptibilities and ESR. Figure 1 shows variable temperature magnetic data for both complexes. The data for the monoclinic form indicate an anomalous magnetic behavior characteristic of an LS⇌HS spin-crossover behavior; the magnetic susceptibility is of an intermediate value at 296 K, and the electronic

state of 40% high-spin and 60% low-spin states. The twin crystals remain fully in the high-spin state, even at 78 K.

ESR spectra were measured for both samples. As the temperature of complex **a** was decreased, the low-spin signals (g_1=2.20, g_2=2.194, g_3=1.944) increased in intensity at the expense of the high-spin signals(g=4 and 2). These high- and low-spin ESR signals are typical for ferric centers of this type. In the twin crystals broad signals at g=2.1, 3.7, and 5.3 were observed at 296 K.

Mössbauer Spectra. The Mössbauer spectra of the monoclinic form were measured at various temperatures (Fig. 2). The spectrum at 78 K is typical of low-spin iron(III); the residual paramagnetic species was not observed, although the magnetic moment (2.58 BM at 80 K) is more than the spin-only value (1.98 BM). The full widths at half maximum(FWHM) at high temperature became broad due to a spin-spin interaction. The spectral data reported in Table 2 characterize anomalous magnetic properties arising from a spin-state interconversion; the spectra are not a superimposition of

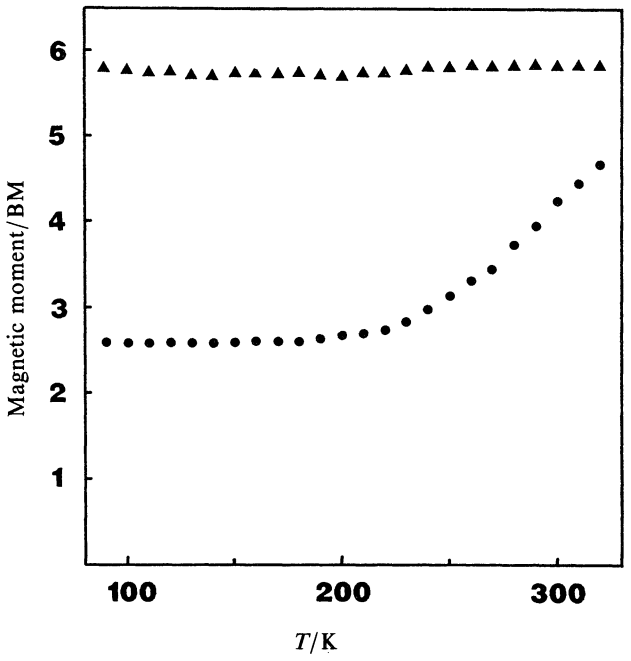

Fig. 1. Temperature dependences of magnetic moments for monoclinic [FeL]BPh_4·acetone (●) and twin crystals (▲).

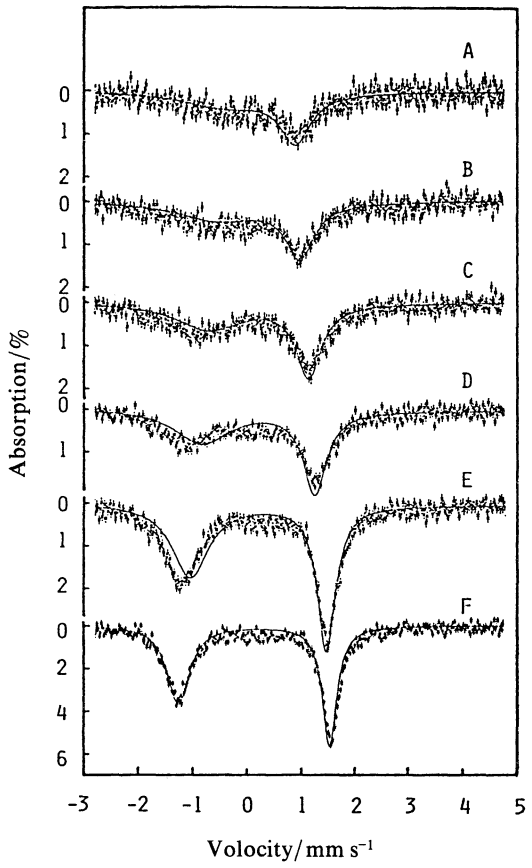

Fig. 2. Temperautre dependence of representative Mössbauer spectra for monoclinic [FeL]BPh_4·acetone and fits. (A) 320 K, $\tau=0.39\times10^{-8}$, f=0.60; (B) 310 K, $\tau=0.47\times10^{-8}$, f=0.53; (C) 296 K, $\tau=0.60\times10^{-8}$, f=0.40; (D) 280 K, $\tau=0.70\times10^{-8}$, f=0.30; (E) 250 K, $\tau=0.87\times10^{-8}$, f=0.13; (F) 200 K, $\tau=0.98\times10^{-8}$, f=0.02.

Table 2. Mössbauer Parameters with Two Lorentzian Lines, High-Spin Fraction and Average Interconversion Rate for Monoclinic [Fe(sal_2trien)]BPh_4·acetone

T	ΔE[a]	δ[b]	Γ_l[c]	Γ_h[d]	χ[e]	f[f]	k'[g]
K	mm s^{-1}	mm s^{-1}	mm s^{-1}	mm s^{-1}		%	s^{-1}
320	1.165	0.364	2.199	0.659	469	60	1.3×10^8
310	1.453	0.286	2.155	0.688	511	53	1.1×10^8
296	1.986	0.168	1.708	0.732	464	40	8.2×10^7
280	2.226	0.170	1.709	0.705	617	30	6.6×10^7
250	2.658	0.153	0.791	0.457	566	13	3.9×10^7
200	2.799	0.164	0.543	0.357	584	2	1.4×10^7
78	2.852	0.223	0.438	0.310	535	0	—

a) Quadrupole splitting. b) Isomer shift relative to metallic iron. c) Full width at half maximum for low energy line. d) Full width at half maximum for high energy line. e) Total of residual sum, free degree is 493. f) High-spin population fraction estimated from the data of magnetic susceptibilities. g) Average interconversion rate tentatively estimated from the Mössbauer fitting.

both high- and low-spin absorptions, but comprise the time-averaged state in both electronic spin-states. The quadrupole splitting values are decreased with increasing population of the high-spin state. These facts indicate that the lifetimes of the low- and high-spin states are as short as or less than the Mössbauer lifetime of ^{57}Fe (1×10^{-7} s).

If we assume that the magnetic moments for low- and high- spin states of the monoclinic crystals are 2.58 and 5.60 BM, respectively, and temperature-independent values are assumed for the low- and high-spin effective magnetic moments, the high-spin population fraction (x) at ambient temperature can be calculated using the $\mu_{obs}^2=x\mu_{hs}^2+(1-x)\mu_{ls}^2$ relation (collected in Table 2).

The relaxation time, τ, is represented by $\tau=\tau_l\tau_h/(\tau_l+\tau_h)$, where τ_l and τ_h are the lifetimes of the low- and high-spin species, respectively. The observed spectra show a rapid relaxation between the high- and low-spin states with the rate of the Mössbauer time scale of 10^{-7} s. Although a fitting is one of many attempts, such a treatment should involve computing the distribution of the relaxation spectra, a correction for the line broadening resulting from the thick absorber and the temperature dependence of the quadrupole splitting for the low-spin species. Such a complex treatment was not attempted herewith and, consequently, the absolute values of the relaxation rate should be taken with caution. Our best fits are illustrated in Fig. 2. The rates for the forward k_1 and reverse k_{-1} rate constants for the spin interconversion LS$\rightleftharpoons$HS are defined as $1/\tau_{ls}$ and $1/\tau_{hs}$, respectively. The low-spin population fraction, f_{ls}, times k_1 is equal to the high-spin fraction, f_{hs}, times k_{-1}, *i.e.*,

$$f_{hs}+f_{ls}=1 \text{ and } k_1f_{ls}=k_{-1}f_{hs}$$

are fulfilled. An equilibrium constant, $K=k_{-1}/k_1$, plot of the temperature-dependent LS$\rightleftharpoons$HS relaxation rates described above deviates from a straight line (Fig. 3); the enthalpy for this process could therefore not be determined accurately. Nonetheless, the fitting of the Mössbauer spectra shown in Fig. 2 can serve as a qualitative of a rapid interexchange system. Sinn et al.[6] have reported that the average rate, $k'=\sqrt{k_1k_{-1}}$, for [FeL]$^+$ in solution is 1.4×10^7 s^{-1} at room temperature. The $\tau=0.6\times10^{-8}$ s in the spectrum (c) of Fig. 2 corre-

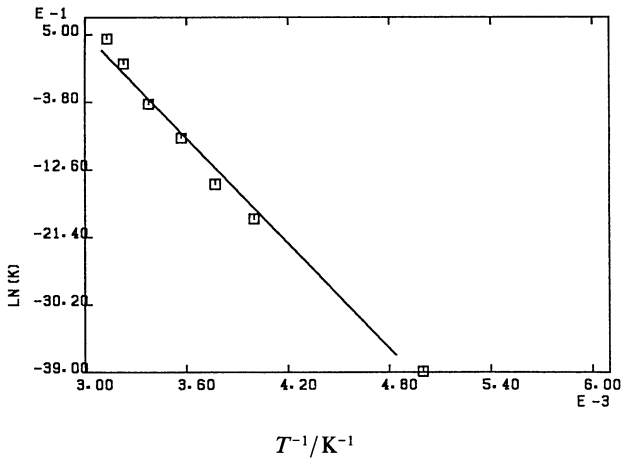

Fig. 3. Plots of natural logarithm of equilibrium constant $K=k_1/k_{-1}$ vs. $1/T$ for monoclinic [FeL]BPh$_4$·acetone (inclination of a straight line is -0.23×10^4 K).

Table 3. Interatomic Distances (Å) for the Cation and Acetone Molecule of Monoclinic [Fe(sal$_2$trien)]BPh$_4$·acetone with Estimated Standard Deviations in Parentheses

Fe–O(1)	1.875(4)	Fe–O(2)	1.875(4)
Fe–N(1)	1.993(4)	Fe–N(2)	2.065(4)
Fe–N(3)	2.073(5)	Fe–N(4)	1.982(5)
O(1)–C(1)	1.326(6)	C(1)–C(2)	1.385(8)
C(2)–C(3)	1.361(8)	C(3)–C(4)	1.385(9)
C(4)–C(5)	1.359(9)	C(5)–C(6)	1.421(7)
C(6)–C(1)	1.420(7)	C(6)–C(7)	1.423(8)
C(7)–N(1)	1.297(6)	N(1)–C(8)	1.474(8)
C(8)–C(9)	1.488(9)	C(9)–N(2)	1.491(7)
N(2)–C(10)	1.506(7)	C(10)–C(11)	1.504(9)
C(11)–N(3)	1.466(8)	N(3)–C(12)	1.441(13)
C(12)–C(13)	1.371(15)	C(13)–N(4)	1.450(10)
N(4)–C(14)	1.293(8)	C(14)–C(15)	1.438(8)
C(15)–C(16)	1.402(8)	C(16)–C(17)	1.349(9)
C(17)–C(18)	1.376(9)	C(18)–C(19)	1.377(9)
C(19)–C(20)	1.410(8)	C(20)–O(2)	1.315(6)
C(20)–C(15)	1.395(7)		

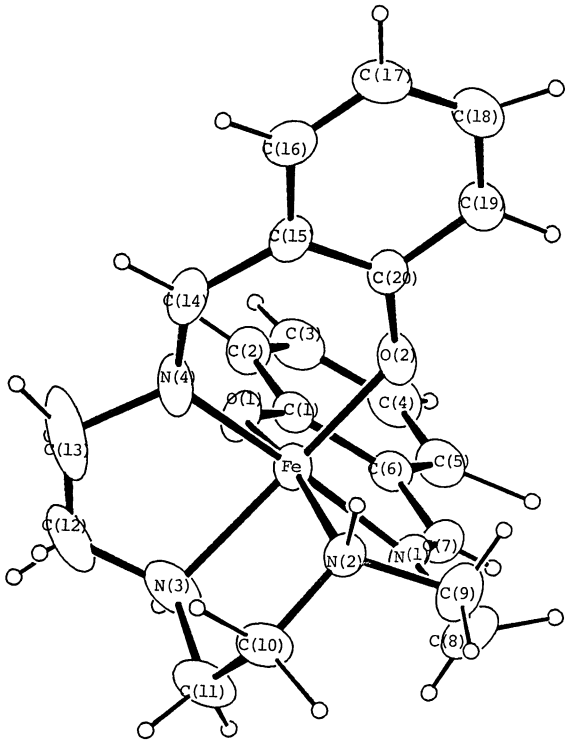

Fig. 4. Ortep figure for the cation of monoclinic [FeL]BPh$_4$·acetone.

sponds to the rate $k'=\sqrt{k_1 k_{-1}}=8.2\times10^7$ s^{-1} and is compared with solution rate. This result is consistent with a report that the spin-state interconversion rates are dependent on the crystal packing and that intermolecular interaction can induce a faster rate than that in an isolated system.[17]

Crystal Structure. The crystal structure of the monoclinic form was determined at 290 K; interatomic distances for the cation and acetone molecule, and bond angles for the cation are listed in Tables 3 and 4, respectively. Steric structure and numbering system for the cation are drawn in Fig. 4 using ORTEP.[18] The structure of the complex contains cation and anion layers in an ac plane, as shown in Fig. 5. The $[FeL]^+$ ion is hydroden bonded via an amine nitrogen (H(23) attached to the nitrogen atom N(2)) to oxygen atom of the

Table 4. Bond Angles (°) for the Cation of Monoclinic [Fe(sal$_2$trien)]BPh$_4$·acetone with Estimated Standard Deviations in Parentheses

O(1)-Fe-O(2)	100.0(2)	O(1)-Fe-N(1)	91.0(2)
O(1)-Fe-N(2)	168.0(2)	O(1)-Fe-N(3)	89.4(2)
O(1)-Fe-N(4)	91.1(2)	O(2)-Fe-N(1)	89.9(2)
O(2)-Fe-N(2)	89.8(2)	O(2)-Fe-N(3)	168.8(2)
O(2)-Fe-N(4)	91.5(2)	N(1)-Fe-N(2)	82.1(2)
N(1)-Fe-N(3)	96.0(2)	N(1)-Fe-N(4)	177.3(2)
N(2)-Fe-N(3)	81.7(2)	N(2)-Fe-N(4)	95.6(2)
N(3)-Fe-N(4)	82.2(2)	Fe-O(1)-C(1)	129.2(3)
O(1)-C(1)-C(2)	119.5(5)	C(1)-C(2)-C(3)	122.1(5)
C(2)-C(3)-C(4)	120.5(6)	C(3)-C(4)-C(5)	119.8(6)
C(4)-C(5)-C(6)	121.0(5)	C(5)-C(6)-C(1)	118.6(5)
C(1)-C(6)-C(7)	123.4(4)	C(6)-C(1)-O(1)	122.4(5)
C(6)-C(1)-C(2)	118.1(5)	C(5)-C(6)-C(7)	118.0(5)
C(6)-C(7)-N(1)	125.3(4)	C(7)-N(1)-C(8)	119.0(4)
C(7)-N(1)-Fe	125.0(4)	Fe-N(1)-C(8)	115.4(3)
N(1)-C(8)-C(9)	107.9(5)	C(8)-C(9)-N(2)	110.9(5)
C(9)-N(2)-C(10)	115.4(4)	C(9)-N(2)-Fe	107.2(3)
Fe-N(2)-C(10)	112.0(3)	N(2)-C(10)-C(11)	109.7(5)
C(10)-C(11)-N(3)	109.7(5)	C(11)-N(3)-C(12)	113.0(5)
C(11)-N(3)-Fe	111.7(4)	Fe-N(3)-C(12)	107.5(5)
N(3)-C(12)-C(13)	121.6(7)	C(12)-C(13)-N(4)	111.7(7)
C(13)-N(4)-C(14)	118.7(5)	C(13)-N(4)-Fe	114.7(4)
Fe-N(4)-C(14)	126.7(4)	N(4)-C(14)-C(15)	124.5(5)
C(14)-C(15)-C(16)	117.3(5)	C(15)-C(16)-C(17)	121.9(5)
C(16)-C(17)-C(18)	118.9(6)	C(17)-C(18)-C(19)	121.1(6)
C(18)-C(19)-C(20)	121.0(5)	C(19)-C(20)-C(15)	117.0(5)
C(20)-C(15)-C(16)	120.1(5)	C(20)-C(15)-C(14)	122.6(5)
C(19)-C(20)-O(2)	118.1(4)	C(15)-C(20)-O(2)	125.0(5)
C(20)-O(2)-Fe	129.2(3)		

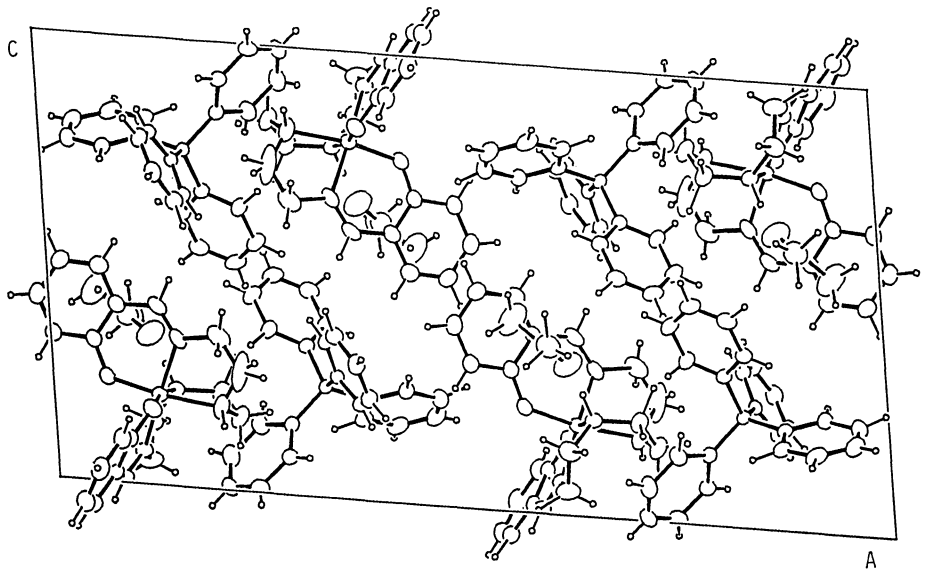

Fig. 5. Packing diagram in ac plane for monoclinic [FeL]BPh$_4$·acetone.

acetone molecule; bond lengths OS(1)–H(23)=2.073 Å, H(23)–N(2)=0.999 Å, OS(1)–N(2)=2.953 Å. The coordination sphere around the iron atom in the cation is approximately octahedral with the two terminal oxygen atom *cis* to each other. The configuration of the hexadentate ligand about the metal atom is analogous to that of low-spin [FeL]NO_3·H_2O (complex **b**) and [FeL]Cl·2H_2O (complex **c**), of which the structures were determined by Sinn et al.[6]; the deviation from octahedral geometry in the FeN_4O_2 unit is larger than those of complexes **b** and **c**. The angles O(1)–Fe–N(2), O(2)–Fe–N(3), and N(1)–Fe–N(4) are 168.0°, 168.8°, and 177.3°, respectively. The iron-ligand bond lengths are Fe–O^{av} 1.875, Fe–N_{imine}^{av} 1.988, and Fe–N_{amine}^{av} 2.069 Å. The Fe–O^{av} bond length for **a** is a little less than those for **b** and **c** 1.885 Å. The Fe–N bond length for **a** is larger than those for **b** and **c**. The bonds to the oxygen atoms are shortest, followed by those to the imine and the amine nitrogen atoms. These bond lengths are less than those for typical high-spin complexes with a Schiff base, in accordance with the electronic spin-state of this complex; i.e. the high-spin population fraction is 40% at 296 K.

With respect to the difference in the bond angles, Fe–O–C, between low-spin [FeL]X(X=NO_3, Cl) and complex **a**, the bond angles of Fe–O(1)–C(1) (129.2°) and Fe–O(2)–C(20) (129.2°) for **a** are about 4° larger than those for **b** or **c** respectively. The difference is larger than those for any other angles; four Fe–N–C angles for **a** are analogous to those corresponding to **b** or **c**. We have pointed out that the ease to transform the Fe–O–C bond angle between both spin-states is important regarding the spin-crossover behavior of FeN_4O_2 Schiff base complexes.[19,20]

The octahedral coordination around an iron atom is stable in the coordination structure represented by Fig. 4; other coordination structures have great strain.[21] Therefore, the coordination structure of twin crystals would be analogous to that shown in Fig. 4, and there would be a faint difference in the molecular structures between the monoclinic- and twin-type crystals.

It is reasonable that the hydrogen bonding interaction produces an increase in the low-spin populations. Complexes **b** and **c** with a strong hydrogen-bonding network are in a low-spin state and, therefore, the electronic states of complex **a** with weak hydrogen bonding and of the desolvated [FeL]BPh_4 may be on the spin-crossover point. It would be very interesting to clarify which difference in the molecular structure in these complexes brings about the spin-state difference. We are now trying to obtain single crystals of the other form (twin crystals).

Desolvated complexes [FeL]BPh_4 are also spin-crossover complexes, and the spin-state interconversion rate is slower than the inverse of the Mössbauer lifetime.[6] It is therefore not necessary to have acetone molecules in the crystal to cause a spin-crossover behavior. Rapid spin-state interconversion may result from the incorporation of acetone molecules, by which any soft modes are devoted to lattice vibration.

Supplementary Materials are Available: Tables of (1) positional parameters except hydrogen atoms, (2) positional parameters for hydrogen atoms, (3) anisotropic temperature factors, (4) mean square displacement tensor for atoms, and (5) observed and calculated structure factors for monoclinic [Fe(sal$_2$trien)]BPh_4·acetone are deposited as Document No. 9110 at the Office of the Editor of Bull. Chem. Soc. Jpn.

References

1) P. Gütlich, *Struct. Bonding (Berlin)*, **44**, 83 (1981).
2) W. R. Scheidt and C. A. Reed, *Chem. Rev.*, **81**, 543 (1981).
3) Y. Maeda and Y. Takashima, *Comm. Inorg. Chem.*, **7**, 41 (1988).
4) E. V. Dose, K. M. Murphy, and L. J. Wilson, *Inorg. Chem.*, **15**, 2622 (1976).
5) M. F. Tweedle and L. J. Wilson, *J. Am. Chem. Soc.*, **98**, 4824 (1976).
6) E. Sinn, G. Sim, E. V. Dose, M. F. Tweedle, and L. J. Wilson, *J. Am. Chem. Soc.*, **78**, 3375 (1978).
7) E. König and K. Medeja, *Inorg. Chem.*, **6**, 48 (1967). P. Ganguli, P. Gütlich, E. W. Müller, and W. Irler, *J. Chem. Soc., Dalton Trans.*, **1981**, 441.
8) B. Gallois, J. A. Real, C. Hauw, and J. Zarembowitch, *Inorg Chem.*, **29**, 1152 (1990).
9) E. König, K. Madeja, and K. J. Watson, *J. Am. Chem. Soc.*, **90**, 1146 (1968).
10) W. R. Scheidt, D. K. Geiger, and K. J. Haller, *J. Am. Chem. Soc.*, **104**, 495 (1982).
11) W. R. Scheidt, D. K. Geiger, R. G. Hayes, and G. Lang, *J. Am. Chem. Soc.*, **105**, 2625 (1983).
12) B. D. Sarma and J. C. Bailar, *J. Am. Chem. Soc.*, **77**, 5476 (1955).
13) J. A. Pople, W. G. Schneider, and H. J. Bernstein, "High Resolution Nuclear Magnetic Resonance," McGraw-Hill, New York (1959); Y. Maeda, Y. Takashima, N. Matsumoto, and A. Ohyoshi, *J. Chem. Soc., Dalton Trans.*, **1986**, 1115.
14) J. A. Ibers and W. C. Hamilton, "International Tables for X-Ray Crystallography," Kynoch Press, Birmingham, England (1974), Vol. IV.
15) R. F. Stewart, E. R. Davidson, and W. T. Simpson, *J. Chem. Phys.*, **42**, 3175 (1965).
16) T. Sakurai and K. Kobayashi, *Sci. Rep. Inst. Chem. Phys. Res. Jpn.*, **55**, 69 (1979).
17) Y. Maeda, M. Tomokiyo, K. Kitazaki, and Y. Takashima, *Bull. Chem. Soc. Jpn.*, **61**, 1953 (1988).
18) C. K. Johnson, ORTEP, Report ORNL-3794, Oak Ridge National Laboratory, Oak Ridge, Tennessee (1965).
19) Y. Maeda, H. Oshio, K. Toriumi, and Y. Takashima, to be published.
20) B. J. Kenedy, A. C. McGrath, K. S. Murray, B. W. Skelton, and A. H. White, *Inorg. Chem.*, **26**, 483 (1987).
21) B. das Sarma and J. C. Bailar, Jr., *J. Am. Chem. Soc.*, **77**, 5476 (1955).